

Adaptive Elastic Networks as models of supercooled liquids

Le Yan, Matthieu Wyart

Center for Soft Matter Research, Department of Physics, New York University
4 Washington Place, New York, 10003, NY, USA

The thermodynamics and dynamics of supercooled liquids correlate with their elasticity. In particular for covalent networks, the jump of specific heat is small and the liquid is strong near the threshold valence where the network acquires rigidity. By contrast, the jump of specific heat and the fragility are large away from this threshold valence. In a previous work (*PNAS*, 110(16):6307, 2013) we could explain these behaviors by introducing a model of supercooled liquids in which local rearrangements interact via elasticity. However, in that model the disorder characterizing elasticity was frozen, whereas it is itself a dynamic variable in supercooled liquids. Here we study numerically and theoretically adaptive elastic network models where polydisperse springs can move on a lattice, thus allowing for the geometry of the elastic network to fluctuate and evolve with temperature. We show numerically that our previous results on the relationship between structure and thermodynamics hold in these models. We introduce an approximation where redundant constraints (highly coordinated regions where the frustration is large) are treated as an ideal gas, leading to analytical predictions that are accurate in the range of parameters relevant for real materials. Overall, these results lead to a description of supercooled liquids in which the distance to a rigidity transition controls the number of directions in phase space that costs energy and the specific heat.

I. INTRODUCTION

Liquids undergo a glass transition toward an amorphous solid state when cooled rapidly enough to avoid crystallization [1]. The glass lacks structural order: it is a liquid “frozen” in one of its inherent structures - local minima in the energy landscape [2], due to the slowing down of relaxation processes. It is very plausible that the thermodynamics and the dynamics in supercooled liquids strongly depend on the microscopic structure associated to these inherent structures. However, a majority of glass theories [3–9] have focused on explaining the correlations between macroscopic observables seen in experiments (such as the relationship between thermodynamics and dynamics [10, 11]), while only a few [12–14] have investigated the role of structure.

Experiments reveal that elasticity is an essential aspect affecting both thermodynamic and dynamical properties in supercooled liquids, such as the jump of specific heat and the fragility characterizing the glass transition: (I) Glasses present an excess of low frequency vibrational modes with respect to Debye modes. The number of these excess soft modes, quantified as the intensity of boson peak [15], shows a strong anti-correlation with the fragility [16, 17]. (II) The rigidity of the inherent structures is tunable by changing the fraction of components with different valences in network glasses [18–20], where atoms interact via covalent bonds and much weaker Van der Waals forces. The covalent network becomes rigid [21–23], when the average valence r exceeds a threshold r_c determined by the balance between the number of covalent constraints and the degrees of freedom of the system. Both the fragility and the jump of specific heat depend non-monotonically on r , and their minima coincide with r_c [18, 24], while no theory [12, 25] has rationalized this

non-monotonicity.

Recently observations [26–30] and theory [31–38] indicate that in various amorphous materials the presence of soft elastic modes is regulated by the proximity of the rigidity transition, linking evidence (I) and (II). To rationalize both (I) and (II), we have introduced a frozen elastic network model which bridges the gap between network elasticity and geometry on the one hand, and the thermodynamics and dynamics of liquids [39]. This model incorporated the following aspects of supercooled liquids: (i) particles interact with each other with interactions that can greatly differ in strength, such as the covalent bonds and the much weaker Van der Waals interactions found in network glasses. (ii) Neighboring particles can organize into a few distinct local configurations. (iii) The choice of local configurations are coupled at different location in space via elasticity. These features were modeled using a random elastic network whose topology was frozen, as illustrated in Fig.2. The possibility for local configurations to change was incorporated by letting the springs switch between two rest length. Despite its simplicity, this model recovered (I) and (II), in particular it reproduced the non-monotonic variance of the jump of specific heat and the fragility with the coordination z of the network, which are extremal at $z_c = 2d$ where a rigidity transition occurs, where d is the spatial dimension. This model could be solved analytically, and led to the view that near the rigidity transition, the jump of specific heat is small because frustration vanishes: most directions in phase space do not cost energy, and thus do not contribute to the specific heat.

This is an novel explanation for a long-standing problem, and it is important to confirm that this view is robust when more realism is brought into the model. In particular, the model used frozen disorder to describe

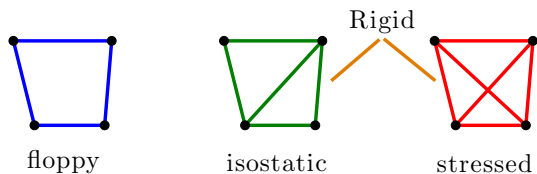


FIG. 1: Illustration of rigidity transition. Blue, green, and red color the floppy, isostatic, and stressed clusters.

elasticity, whereas it is itself a dynamical property in liquids, where there cannot be any frozen disorder. The thermal evolution of the topology of the contact network and its effects on rigidity transition were also not addressed. A network is rigid when an imposed global strain induces stress, and the rigidity can be achieved topologically by adding constraints [21], see Fig. 1 for an illustration in a small network. The network is said to be self-stressed if some of constraints are redundant, removing those leaves the network rigid. Three scenarios of rigidity transition have been extensively studied in the literature [40, 41] (but see [42] for a recent fourth proposition). Spatial fluctuations of coordination are important in the first two. The *rigidity percolation* model [43–46] assumes that bonds are randomly deposited on a lattice. Fluctuations lead to over-constrained (self-stresses) clusters even when the average coordination number is not sufficient to make the whole network rigid. This model corresponds to the infinite temperature limit. To include these effects, self-organized network models were introduced [47–50], where overconstrained regions are penalized. A surprising outcome of these models is the emergence of a rigidity window: rigidity emerges at a coordination number lower than the one where self-stress appears even in the thermodynamic limit. Finally, in the *mean-field or jamming scenario*, fluctuations of coordinations are limited. Similar to the simple picture in Fig. 1, the rigidity and the stress appear at the same z_c in the thermodynamic limit. The rigid cluster at z_c is not fractal, and is similar to that of packings of repulsive particles. The model of [39] assumed that networks where of this last type.

Recently, we have introduced adaptive elastic network models [40], where the topology of the network is free to evolve to lower its elastic energy as the system is cooled. We found that as soon as weak interactions are present, the network of strong interactions become mean-field like at low temperature. However, the thermodynamic properties were not studied to test the robustness of the thermodynamic predictions of [39] relating structure to the jump of specific heat. In this work, we directly show numerically and theoretically that the prediction for the jump of specific heat is essentially identical in adaptive and frozen elastic network models. Section II describes the adaptive network models. Section III presents the numerical results of the model, while Section

IV gives the explicit derivation of the thermodynamics properties, developing an approximation scheme to deal with the temperature-dependence of the number of over-constraints in the system, treating them as an ideal gas.

II. MODEL

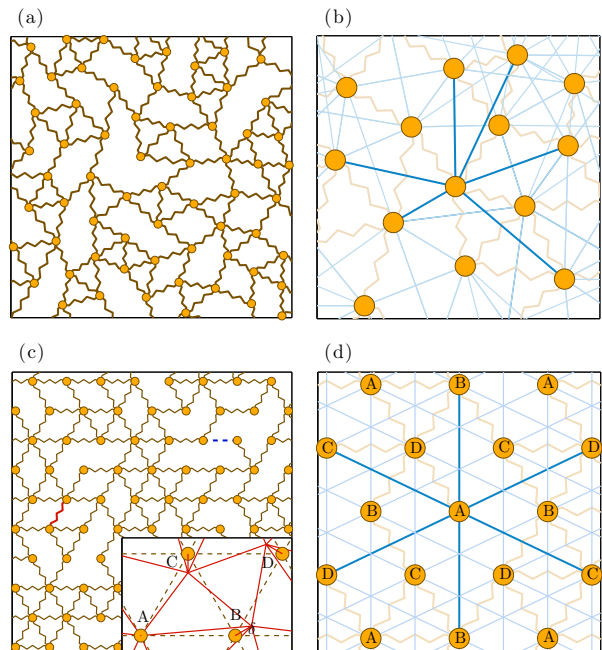


FIG. 2: (a) and (b) Illustration of the frozen network model [39], (c) and (d) the adaptive network model [40]. In that case, the triangular lattice is systematically distorted in a unit cell of four nodes shown in the inset of (c). We group nodes by four, labeled as A B C D in Fig. 2. One group form the unit cell of crystalline lattice. Each cell is distorted identically in following way: node A stays, while nodes B, C, and D move by a distance δ , B along the direction perpendicular to BC, C along the direction perpendicular to CD, and D along the direction perpendicular to DB. δ is set to 0.2 with the lattice constant as unity. Weak springs connecting (b) six nearest-neighbors without strong springs and (d) six next-nearest-neighbors are indicated in cyan lines, emphasized for the central node. (c) illustrates an allowed step, where the strong spring in red relocates to a vacant edge indicated by a blue dashed line.

In our model degrees of freedom are springs, which are poly-disperse and can move on a lattice. The lattice is built using a triangular lattice with periodic boundary conditions, see Fig. 2(c), with a slight regular distortion to avoid straight lines as illustrated in the inset of Fig. 2(c). Polydisperse and mobile “strong” springs of identical stiffness k connect the nearest neighbors on the lattice and model the covalent constraints. We

model weak Van der Waals interactions with “weak” and stationary springs of stiffness $k_w \ll k$ adding to all next-nearest-neighbors on the triangular lattice, illustrated in Fig. 2(b). We introduce a control parameter $\alpha \equiv (z_w/d)(k_w/k)$ to characterize the relative strength of the weak interactions, where the spatial dimension is $d = 2$ and the number of weak constraints per node is chosen $z_w = 6$.

The number of “covalent” springs N_s , equivalent to the coordination number $z \equiv 2N_s/N$ (N is the number of nodes in the lattice), is also a dimensionless control parameter. For a given z , the valid configurations are defined by the locations of the N_s springs, indicated as $\Gamma \equiv \{\gamma \leftrightarrow \langle i, j \rangle\}$, where the Greek index γ labels springs and the Roman indices $\langle i, j \rangle$ label the edges on triangular lattice between nodes i and j . We introduce the variable $\sigma_{\langle i, j \rangle} = 0$ if there is no strong spring on the edge ij , and $\sigma_{\langle i, j \rangle} = 1$ if there is one. If $r_{\langle i, j \rangle}$ denotes the length between nodes i and j on the lattice, we assume that the spring γ has a rest length $l_\gamma = r_{\langle i, j \rangle} + \epsilon_\gamma$, where the mismatch ϵ_γ is a feature of a given spring. ϵ_γ are sampled independently from a Gaussian distribution with mean zero and variance ϵ^2 , which thus characterizes the polydispersity of the model. $k\epsilon^2$ is set to unity as the natural energy scale.

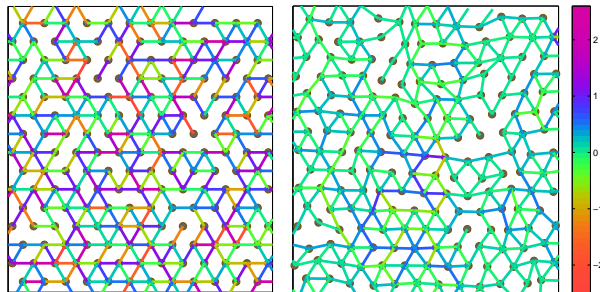


FIG. 3: Illustration of configuration energy of the adaptive network model ($\delta z = 0.27$). Left: Particles sit at their initial lattice sites, links are colored according to their length mismatches of springs to the initial particle distances. From red to purple, the rest length is from shorter to longer than the particle distance. Right: Particles are relaxed to mechanical equilibrium, and most links turn to green, indicating little mismatch between the spring rest length and particle distance.

The energy of an inherent structure is denoted $\mathcal{H}(\Gamma)$. The configuration Γ is sampled with probability proportional to $\exp(-\mathcal{H}(\Gamma)/T)$ in the liquid phase, with $k_B = 1$. Temperature T serves as a third dimensionless control parameter. $\mathcal{H}(\Gamma)$ is defined as the remaining energy once the nodes of the network are allowed to relax to mechan-

ical equilibrium:

$$\mathcal{H}(\Gamma) = \min_{\{\vec{R}_i\}} \left\{ \sum_{\gamma} \frac{k}{2} \left[\|\vec{R}_i - \vec{R}_j\| - l_\gamma \right]^2 + \sum_{\langle i, j \rangle_2} \frac{k_w}{2} \left[\|\vec{R}_i - \vec{R}_j\| - r_{\langle i, j \rangle_2} \right]^2 \right\} \quad (1)$$

where \vec{R}_i is the position of particle i and $\langle i, j \rangle_2$ labels the next-nearest neighbors. The minimal energy can be calculated by steepest decent as illustrated in Fig. 3, which is however computationally expensive. Instead, we approximate the elastic energy in the linear response range, assuming that $\epsilon^2 \ll 1$ [51]. The above minimization expression Eq.(1) could then be written as,

$$\mathcal{H}(\Gamma) = \frac{k}{2} \sum_{\Gamma} \epsilon_{\langle i, j \rangle} \mathcal{G}_{\langle i, j \rangle, \langle l, m \rangle} \epsilon_{\langle l, m \rangle} + o(\epsilon^3) \quad (2)$$

where $\epsilon_{\langle i, j \rangle} = \epsilon_\gamma$ when spring γ connects i and j . The coupling matrix $\mathcal{G} = \mathcal{P} - \mathcal{S}(\mathcal{S}^t \mathcal{S} + \frac{k_w}{k} \mathcal{S}_w^t \mathcal{S}_w)^{-1} \mathcal{S}^t$, derived in our previous works [39, 40] (or see Supplemental Materials Sec. A [52]), is a product of the structure matrix \mathcal{S} and its transpose \mathcal{S}^t , the structure matrix of the weak spring network \mathcal{S}_w , and \mathcal{P} the projection operator of the triangular lattice onto occupied edges. The structure matrices \mathcal{S} and \mathcal{S}_w describe the topology of the networks of strong and weak springs: if neighbor nodes i and j are connected, the change of the distance between i and j , $\delta r_{\langle i, j \rangle} = \mathcal{S}_{\langle i, j \rangle, i} \cdot \delta \vec{R}_i + \mathcal{S}_{\langle i, j \rangle, j} \cdot \delta \vec{R}_j + o(\delta \vec{R}^2)$, due to displacements of nodes $\delta \vec{R}$. We point out that as the weak network is fixed, \mathcal{S} and thus \mathcal{G} depend only on the network topology of strong springs, but not on the mismatches ϵ_γ .

Our model is a generalization of on-lattice network models: setting $\alpha = 0$, it naturally recovers the randomly diluted lattice model [46] when $T = \infty$. It is also related to the self-organized lattice model [47, 48], which postulates that elastic energy is linearly proportional to the number of redundant constraints [47, 53]. We will find that this assumption holds true for $\alpha = 0$ and $T \ll 1$. However real physical systems have $\alpha > 0$ which turns out to completely change the physics, an effect that our model can incorporate.

III. NUMERICS

We implement a Monte Carlo simulation to sample the configuration space of the model, with 10^6 Monte Carlo steps at each T . At each step, a potential configuration is generated by a Glauber dynamics - moving one randomly chosen spring to a vacant edge, as illustrated in Fig. 2(c). We numerically compute the elastic energy of the proposed configuration using Eq.(2): calculating the

structure matrix \mathcal{S} and then the corresponding \mathcal{G} . In the matrix division involved in computing \mathcal{G} , the inverting matrix is singular when the network includes floppy modes, which do not appear except $k_w = 0$. When $\alpha = 0$, we implement the “pebble game” algorithm [54] to identify the over-constrained sub-networks, and then do matrix division in the subspace, as the isostatic and floppy regions store no elastic energy after relaxation. We have found little finite size effect by varying the system size from $N = 64$ to $N = 1024$ nodes in triangular lattice. In the following, we present our numerical results of networks with $N = 256$ nodes, averaged over 50 realizations of random mismatches if not specified.

A. Dynamics

We investigate the dynamics by computing the correlation function $C(t) = \frac{1}{N_s(1-N_s/3N)} (\langle \sigma(t) | \sigma(0) \rangle - N_s^2/3N)$, which decays from one to zero at long time. We define the relaxation time τ as the time $C(\tau) = 1/2$, and the numerical results of τ as a function of temperature T for several different coordination numbers are shown in the Fig. 4.

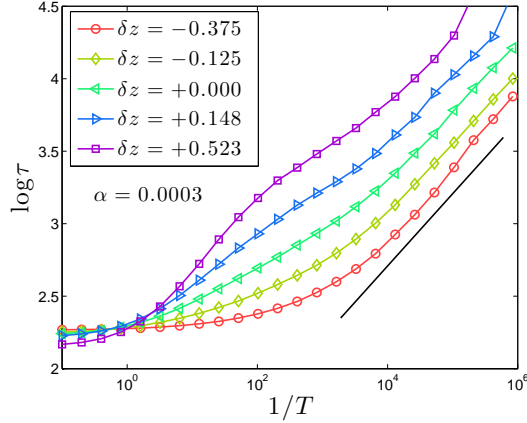


FIG. 4: Relaxation time τ in log-scale versus inverse temperature $1/T$ for different coordination numbers δz and $\alpha = 0.0003$. The black solid line indicates a power law relation between τ and T : $\tau \sim T^{-1/2}$.

We find that the implemented dynamics is not glassy. The relaxation time increases as a power law of the temperature $T^{-0.5}$, even much slower than a strong glass that would display an Arrhenius behavior $\log \tau \propto 1/T$. This result is very surprising, because the frozen elastic network model we studied earlier was glassy (its fragility was similar to that of network liquids). Despite being very different dynamically, these two models are almost identical as far as thermodynamics is concerned, as we will see below. It could be that the lack of glassiness comes from our choice of Monte-Carlo where springs can

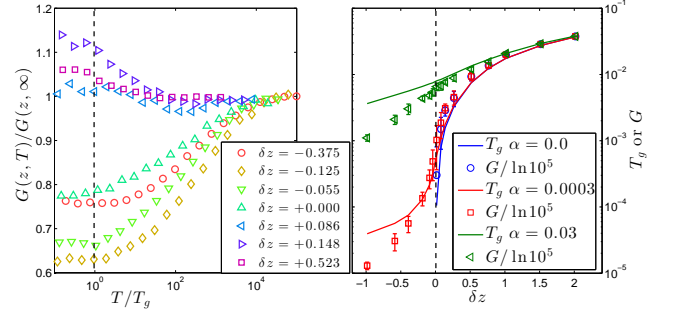


FIG. 5: Left: Shear modulus of adaptive networks at temperature T rescaled by G at $T = \infty$ $G(z, T)/G(z, \infty)$, $\alpha = 0.0003$. The temperature T is rescaled by T_g . Right: Correlation between transition temperature T_g and shear modulus G in the frozen network model [39], shown for different z and α .

try other locations anywhere in the system (it would be interesting to see if similar Monte-Carlo methods used in real models of polydisperse particles can achieve rapid equilibration).

To compare the thermodynamics of these models we now need to define an effective glass temperature T_g (even if we do not see a real glass transition). We do that by using the Lindemann criterion [55] that an amorphous solid melts when the standard deviation $\langle \delta R^2 \rangle^{1/2}$ of particles’ displacement is greater than a fraction $c \approx 0.15$ of the particle size a . We can estimate this standard deviation via the elastic modulus if we treat the glass as a continuum $\langle \delta R^2 \rangle \sim T/Ga$ where G is the shear modulus. we thus get $T_g \propto Ga^3$. We set the lattice length a in our model to unity.

We thus measure the shear modulus averaging over configurations at given temperatures, shown in the left panel of Fig. 5. Practically, we define $T_g = \langle G \rangle_{T_g} / \ln 10^3$. $\langle \bullet \rangle_{T_g}$ is the mean value at temperature T_g . The prefactor in this definition is arbitrary, but its choice does not affect qualitatively our conclusions. The specific values of T_g following that definitions are shown in the inset of the bottom panel of Fig. 7.

Note that this definition of T_g is consistent with the dynamics in the frozen model, as shown in the right panel of Fig. 5 by lining up G [56] and T_g (which can be defined from the dynamics in that case [39]).

B. Specific heat

The specific heat data shown in Figs. 6 and 7 are our central numerical results. The energy $E = \langle \mathcal{H} \rangle$ is obtained using an time-average over Monte Carlo steps, and is shown in Fig. 6(a). The specific heat is calculated as its derivative $c \equiv \frac{1}{N_s} dE/dT$, and is shown versus T for several coordination numbers when $\alpha = 0$ in Fig. 6(b) and $\alpha = 0.0003$ in the top panel of Fig. 7. When $\alpha = 0$, the

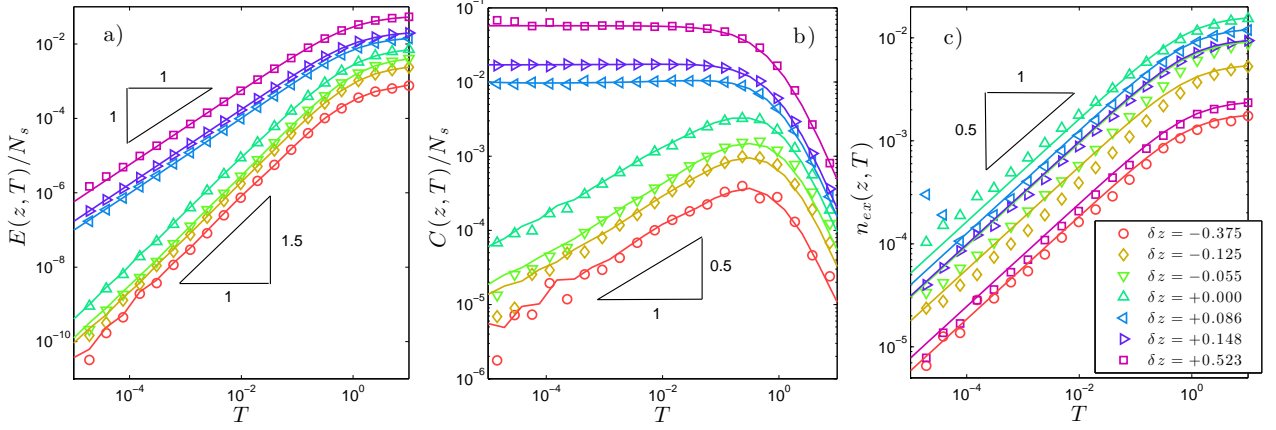


FIG. 6: Thermodynamics of the adaptive network model without weak constraints $\alpha = 0$. (a) Energy E/N_s vs temperature; (b) Specific heat C/N_s vs temperature; (c) Excess number of redundant constraints density n_{ex} extracted using the pebble game algorithm vs temperature. Symbols are numerical data, solid lines are theoretic predictions.

specific heat increases as temperature decreases for networks with $\delta z > 0$ while it meets a maximum at $T_a \sim 1$ and decreases under cooling when $T < T_a$ if $\delta z \leq 0$. In contrast, the specific heat increases under cooling close to the transition temperature for all coordination numbers when $\alpha > 0$. In addition, when $T \lesssim \alpha$, $c \rightarrow 0.5$. All these results are qualitatively identical to our previous frozen model.

To define the jump of the specific heat at the glass transition, we simply measure the specific heat at our glass transition T_g defined above. This definition is natural since in a real glassy system, below T_g the liquid is essentially frozen in an inherent structure, and the contribution to the specific heat from configurational entropy (i.e. the bottom energy of inherent structures) vanishes.

Our central numerical result is shown in the bottom panel of Fig. 7: $c(T_g)$ varies non-monotonically with the coordination number z when $\alpha > 0$. When the network of strong springs is poorly coordinated $\delta z \lesssim 0$, $c(T_g)$ decreases as z increases; When the strong network gets better coordinated $\delta z \gtrsim 0$, c gradually changes to increase with z ; c is minimal at the proximity of the rigidity transition z_c for finite α . These numerical results are very similar to empirical observations, see point (II) in the introduction. Our data are in fact very similar to that of the frozen model, which essentially follows the dotted lines in Fig. 7.

C. Number of redundant constraints R

When $\alpha = 0$ $T \rightarrow 0$, the specific heat is simply proportional to R , as shown in Fig. 6(b). This number is fixed, $R = N\delta z/2$, in the frozen network models. It varies in the adaptive network model, and depends on the temperature. As the Maxwell counting give the minimal number

of redundant constraints of a network, we can define an excess number of redundant constraints

$$n_{ex} \equiv \frac{1}{N_s} \left(R - \frac{N\delta z}{2} \Theta(\delta z) \right), \quad (3)$$

where $\Theta(x)$ is Heaviside step function. n_{ex} counts the average number of redundant constraints additional to the Maxwell counting. This excess number of redundant constraints decreases monotonically to zero under cooling. When $\alpha = 0$, n_{ex} is proportional to \sqrt{T} in the adaptive network model at low temperature, shown in Fig. 6(c).

IV. THEORY

As illustrated in Fig. 8, in the frozen elastic model we found that as $\alpha \rightarrow 0$, c converges to a constant if $z < z_c$, whereas it behaves as $z - z_c$ for $z > z_c$. When α increases, this discontinuous behavior becomes smooth, and looks similar to experimental data. We seek to derive these same features in the adaptive network models.

A. Thermodynamics

For simplicity, we consider the annealed free energy $\mathcal{F}_{ann} = -T \ln \overline{\mathcal{Z}}$. It is exact in random energy model [57] above the ideal glass transition [58] and we find it a good approximation of $\overline{\mathcal{F}}$ in our models [39]. The over-line implies an average over disorder ϵ ,

$$\overline{\mathcal{Z}} = \sum_{\{\sigma\}} \sum_{\text{perm}[\gamma]} \exp[-\mathcal{H}(\Gamma)/T] \quad (4)$$

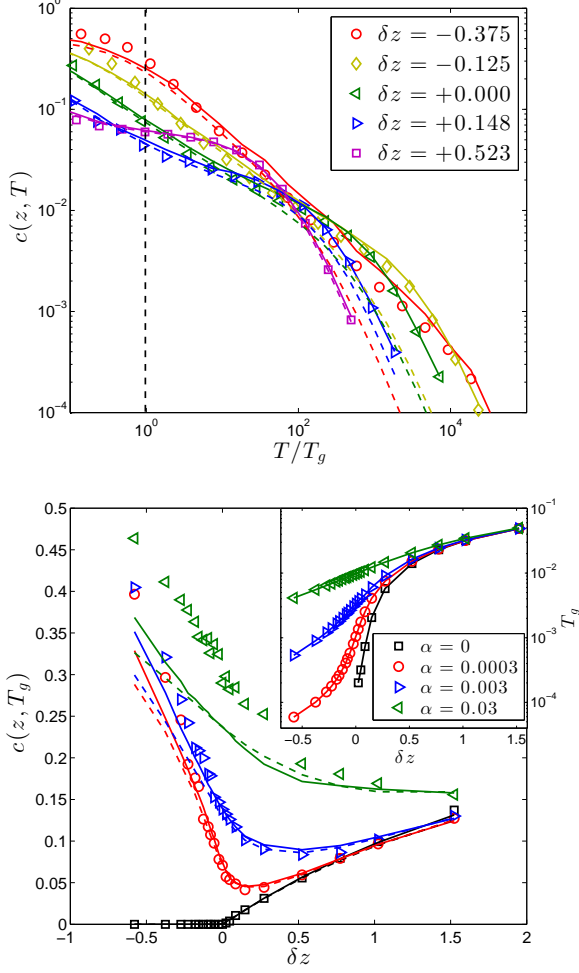


FIG. 7: Top: Specific heat $c(z, T)$ vs scaled temperature T/T_g for networks with average coordination numbers near and away from the isostatic on both floppy and rigid sides. The strength of the weak constraints is given by $\alpha = 0.0003$. Bottom: Specific heat at temperature T_g $c(z, T_g)$ vs coordination number δz for $\alpha = 0, 0.0003, 0.003, 0.03$. The inset shows the transition temperature T_g for different z and α . Symbols are numerical results, and lines are theoretical predictions: dashed lines are for frozen network model and solid lines are for the new model derived in section IV.

where a given configuration Γ is characterized by $\{\sigma\}$ indicating which edges are occupied on the triangular lattice, and $\text{perm}[\gamma]$ labels the different possible permutations of springs rest lengths.

We first average over the quenched randomnesses. Us-

ing the linear approximation Eq.(2) and the Gaussian distribution $\rho(\epsilon_\gamma) = \frac{1}{\sqrt{2\pi\epsilon^2}} e^{-\epsilon_\gamma^2/2\epsilon^2}$,

$$\bar{Z} = \sum_{\{\sigma\}} \left(\frac{Nz}{2} \right)! \exp \left[-\frac{1}{2} \text{tr} \ln \left(\mathcal{I} + \frac{\mathcal{G}(\{\sigma\})}{T} \right) \right] \quad (5)$$

The factorial comes from $N_s! = \sum_{\text{perm}[\gamma]} \mathbf{1}$ as \mathcal{G} is inde-

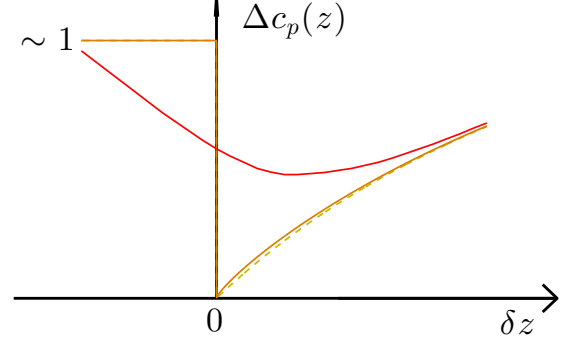


FIG. 8: Theoretical predictions for the jump of specific heat. For vanishingly small weak springs $\alpha \rightarrow 0$, it is predicted that the jump is essentially constant for $z < z_c$ and then drops to zero at z_c . For larger z it behaves as $z - z_c$. As α grows this sharp curve becomes smooth, but a minimum is still present near $z = z_c$.

pendent of the permutation. \mathcal{I} is a $3N \times 3N$ identity matrix; each component corresponds to an edge on the lattice. To compute the trace in the exponent, we first make the approximation that the weak springs are weak and numerous $\mathcal{S}_w^t \mathcal{S}_w \approx \frac{z_w}{d} \mathcal{I}_{Nd \times Nd}$, which corresponds to the highly connected limit $z_w \rightarrow \infty$ and finite α . We can then decompose the coupling matrix $\mathcal{G} \approx \mathcal{P} - \mathcal{S}(\mathcal{S}^t \mathcal{S} + \alpha \mathcal{I})^{-1} \mathcal{S}^t$ as [39]:

$$\mathcal{G}(\{\sigma\}) = \sum_{p(\{\sigma\})} |\psi_p\rangle \langle \psi_p| + \sum_{\omega(\{\sigma\}) > 0} \frac{\alpha}{\omega^2 + \alpha} |\psi_\omega\rangle \langle \psi_\omega| \quad (6)$$

where p labels the vectors $|\psi_p\rangle$ satisfying $\mathcal{S}^t |\psi_p\rangle = 0$ (i.e. a basis for the kernel of \mathcal{S}^t), and where the $|\psi_\omega\rangle$ satisfy $\mathcal{S} \mathcal{S}^t |\psi_\omega\rangle = \omega^2 |\psi_\omega\rangle$. The number of redundant directions is $\sum_p \mathbf{1} = N_s - (Nd - F) \equiv R$. Note that $\text{tr} \mathcal{P} = N_s$, $Nd - F$ gives the number of frequencies ω , and F counts the number of floppy modes. The modes $|\psi_p\rangle$, $|\psi_\omega\rangle$, R and ω depend on occupation $\{\sigma\}$. As the $|\psi\rangle$'s are orthonormal, the trace in Eq.(5) gives

$$\bar{Z} = \left(\frac{Nz}{2} \right)! \sum_{n_r, D(\omega)} \exp \left[N_s \left(s(n_r, D(\omega)) - \frac{n_r}{2} \ln \left(1 + \frac{1}{T} \right) - \frac{1 - n_r}{2} \int d\omega D(\omega) \ln \left(1 + \frac{1}{T} \frac{\alpha}{\omega^2 + \alpha} \right) \right) \right], \quad (7)$$

where $s(n_r, D(\omega)) \equiv \frac{1}{N_s} \ln \sum_{\{\sigma\}} \mathbf{1}_{R, D(\omega)}$ is configura-

tional entropy density with given number of redun-

dant constraints $n_r \equiv R/N_s$ and density of states $D(\omega)$ of vibrational modes, $(1 - n_r) \int d\omega D(\omega) \equiv \lim_{N \rightarrow \infty} \frac{1}{N_s} \sum_{\omega > 0}$.

B. No weak interactions

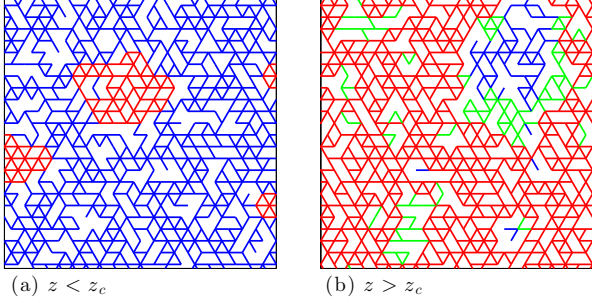


FIG. 9: (a) $z < z_c$, localized redundant constraints (red) in a floppy sea (blue); (b) $z > z_c$ localized floppy modes (blue) in a rigid sea (red and green).

Neglecting the weak constraints $\alpha = 0$, the last term in the exponential vanishes and the summation over states with given density of states can be absorbed into the entropy, which then depends only on the number of redundant constraints.

$$\bar{Z} = \left(\frac{Nz}{2}\right)! \sum_{n_r} e^{N_s[s(n_r) - \frac{n_r}{2} \ln(1 + \frac{1}{T})]} \quad (8)$$

We propose an ideal-gas picture of “defects” to find an approximation form of the entropy $s(n_r)$. When the coordination number is very small $z < z_c$ and the network is mostly floppy, redundant constraints are localized rigid islands. Similarly, when the coordination number is very large $z > z_c$ with most regions of the network rigid, there are localized floppy modes in regions where there is a negative fluctuation of coordination, which we again described as defect, see illustration in Fig. 9. The number of such floppy modes is equal to the number of additional over constrained in the rigid cluster. The entropy gains from having these defects. Assuming that such defects are independent, we approximate the entropy by that of an ideal gas:

$$s(n_{ex}) \approx s(0) - n_{ex} \ln \frac{n_{ex}}{en_0(z)} \quad (9)$$

where n_{ex} is the excess number of redundant constraints defined in Eq.(3), and is thus counting the number of defects. $s(0)$ is the entropy density of the states with a minimal number of redundant constraints (i.e. they satisfy the Maxwell counting); and $n_0(z)$ is the excess number of redundant constraints at $T = \infty$. Both $s(0)$ and n_0 depend only on z and the lattice structure. This

form Eq.(9) should fails when the assumption of independent “defects” breaks down, as must occur near the rigidity transition. However, our numerical results indicate that this approximation is very accurate, we see deviations only for $|\delta z| \lesssim 0.1$.

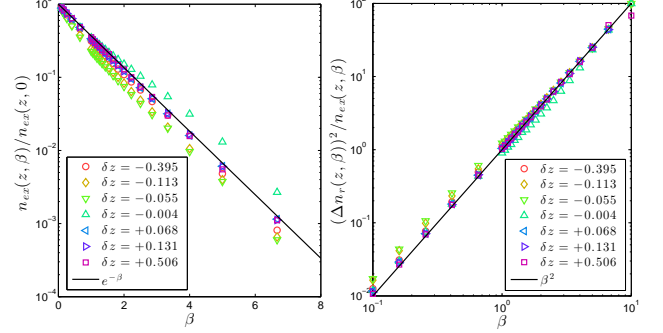


FIG. 10: Left: Excess number of redundant constraints density $n_{ex}(z, \beta)$. Right: Fluctuation of the number of redundant constraints density $(\Delta n_r)^2$. The black solid lines show the predictions from the approximate entropy Eq.(9).

We numerically test the formula Eq.(9) for a triangular lattice. The configurations with R redundant constraints are weighted by $e^{-\beta R}$ for different parameter β . Derived from Eq.(9), the mean and variance of the excess number of redundant constraints density depending on β satisfy the following formulae:

$$\beta \equiv \frac{\partial s}{\partial n_{ex}} \Rightarrow n_{ex}(z, \beta) = n_0(z) e^{-\beta} \quad (10a)$$

$$\Delta n_{ex}^2(z, \beta) = -\beta^2 \frac{\partial}{\partial \beta} n_{ex}(z, \beta) = \beta^2 n_{ex}(z, \beta) \quad (10b)$$

Our numerical results coincide with Eqs.(10a) and (10b) remarkably well, with minor deviations for $|\delta z| \lesssim 0.1$.

Applying Eq.(9), we derive the thermodynamics of our model when $\alpha = 0$. Solving the saddle point of Eq.(8), we obtain the average energy density:

$$\frac{1}{N_s} E(z, T) = \frac{r_0 + n_{ex}(z, T)}{2} \frac{T}{1 + T} \quad (11a)$$

the specific heat:

$$\frac{1}{N_s} C(z, T) = \frac{r_0 + \frac{3}{2} n_{ex}(z, T)}{2} \frac{1}{(1 + T)^2} \quad (11b)$$

and the density for the excess number of redundant constraints:

$$n_{ex}(z, T) = n_0(z) \left(1 + \frac{1}{T}\right)^{-1/2} \quad (11c)$$

where $r_0 \equiv \frac{\delta z}{z} \Theta(\delta z)$.

As $n_0(z)$ is expected to be an analytic function of z , Eqs.(11) indicate that c converges to the one found in frozen network model in the limit $T \rightarrow 0$: $c = 0$ when $\delta z < 0$ and $c = \delta z/2z$ when $\delta z > 0$ - the yellow dashed line in Fig. 8. This is one of our central result, showing that our previous results hold even when the network is adaptive.

Eqs.(11) predict the energy, specific heat, and the number of redundant constraints at an arbitrary temperature without any fitting parameter. The solid lines shown in Fig. 6(a,b) are predictions of Eqs.(11a) and (11b) with n_{ex} as the numerical input. They are closely consistent with the data points, which confirms the annealed free energy approximation when $\alpha = 0$. A $T^{1/2}$ power-law with numerical prefactor $n_0(z) = n_{ex}(z, \infty)$ predicted by Eq.(11c) coincides well with data points in Fig. 6(c).

Extending to finite glass transition T_g at $\alpha = 0$, we find a correction vanishing as $\sqrt{\delta z}$ in addition to $c \approx \delta z/2z$, assuming $T_g \sim G \sim \delta z$ for $z > z_c$. But this correction is quantitatively unimportant as $n_0 \leq 0.03$ and does not change qualitatively the linear growth of the specific heat when $\delta z > 0$, as illustrated by the orange solid line in Fig. 8.

Our theoretic prediction that $n_{ex} \rightarrow 0$ when $T \rightarrow 0$ validates the assumptions of [47, 48, 53] that the energy of redundant bonds is proportional to their number, and that this number is R_0 at $T = 0$.

C. General case

In the thermodynamic limit $N_s \rightarrow \infty$, we take the saddle point of Eq.(7),

$$\frac{2\delta s}{\partial n_r} = \ln\left(1 + \frac{1}{T}\right) - \int d\omega D(\omega) \ln\left(1 + \frac{1}{T} \frac{\alpha}{\omega^2 + \alpha}\right) \quad (12a)$$

and

$$\frac{2\delta s}{\delta D(\omega)} = (1 - n_r) \ln\left(1 + \frac{1}{T} \frac{\alpha}{\omega^2 + \alpha}\right) \quad (12b)$$

and solving for energy,

$$\begin{aligned} \frac{1}{N_s} E(z, T, \alpha) &= \frac{n_r(T)}{2} \frac{T}{1+T} \\ &+ \frac{1 - n_r(T)}{2} \int d\omega D(\omega, T) \frac{\alpha T}{\alpha + (\omega^2 + \alpha)T} \end{aligned} \quad (13)$$

The specific heat predictions from differentiating Eq.(13) with numerical inputs $n_r(z, T, \alpha)$ and $D_{z,T,\alpha}(\omega)$ are plotted as solid lines in Fig. 7. (See Supplemental Materials Secs. BCD for the temperature dependence of $D(\omega)$.) Notice that replacing $n_r(T)$ by $\delta z/z$ and $D(\omega, T)$ by its low-temperature limit $D(\omega)$ studied in [39, 59, 60], Eq.(13) recovers exactly the one obtained in the frozen

network model, whose predictions are plotted as dashed lines in Fig. 7. The dashed lines converge to the solid lines despite differences at high temperatures for weakly coordinated networks.

In the limit $\alpha \rightarrow 0$ and $T \ll \alpha$, Eq.(13) converges to $E/N_s = T/2$, which indicates a constant specific heat $c = 0.5$ when $\delta z < 0$ independent of the models. This is shown by the orange solid line and the yellow dashed line in Fig. 8, and is our second key theoretical result showing the robustness of our conclusions for adaptative networks.

V. CONCLUSIONS

In this work, we have studied the correlation between the elasticity of inherent structures and the thermodynamics in covalent glass-forming liquids using adaptive network models. We found numerically and explained theoretically why these model have a thermodynamic behavior similar to frozen network models [39] which captures nicely experimental facts. Note that we have focused on the configurational part of the jump of specific heat, since we considered only the energy minima in the metastable states. However in Supplemental Materials Sec. E we argue that the vibrational contribution to this jump is quite small in our models.

We thank E. DeGiuli, G. Düring, E. Lerner, J. Lin, C. Sandford for discussions, and D. Jacobs for sharing the pebble game code. This work has been supported primarily by the National Science Foundation CBET-1236378, and partially by the Sloan Fellowship, the NSF DMR-1105387, and the Petroleum Research Fund 52031-DNI9.

SUPPLEMENTAL MATERIALS: ADAPTIVE ELASTIC NETWORKS AS A MODEL FOR SUPERCOOLED LIQUIDS

A. Formalism of elastic energy

The energy $H(\Gamma)$ of a given spring configuration $\Gamma \equiv \{\gamma \leftrightarrow \langle i, j \rangle\}$ is defined in Eq.(1) of the main text as a minimization on the positions of the nodes. This minimum can be calculated using conjugate gradient methods. However for small mismatches ϵ , it is more efficient to use linear algebra [39], as we now recall. Consider a displacement field $\delta \vec{R}_i \equiv \vec{R}_i - \vec{R}_{i0}$, where \vec{R}_{i0} is the position of the node i in the crystal described in the previous section. We define the distance $\|\vec{R}_{i0} - \vec{R}_{j0}\| \equiv r_{\langle i, j \rangle}$. At first order in $\delta \vec{R}_i$, the distance among neighboring nodes can be written as:

$$\|\vec{R}_i - \vec{R}_j\| = r_{\langle i, j \rangle} + \sum_k \mathcal{S}_{\langle i, j \rangle, k} \delta \vec{R}_k + o(\delta \vec{R}^2) \quad (S1)$$

Where \mathcal{S} is the structure matrix, which gives the linear relation between displacements and changes of distances, as indicated in Eq.(S1). Minimizing Eq.(1) in the main text, one gets:

$$H(\Gamma) = \min_{\{\delta \vec{R}_i\}} \left\{ \frac{k}{2} \sum_{\gamma} \left(\sum_i \mathcal{S}_{\gamma,i} \delta \vec{R}_i + \epsilon_{\gamma} \right)^2 + \frac{k}{2} \sum_{\sigma} \frac{k_w}{k} \left(\sum_i \mathcal{S}_{w,\sigma,i} \delta \vec{R}_i \right)^2 + o(\delta \vec{R}^3) \right\} \\ = \min_{\{\delta \vec{R}_i\}} \frac{k}{2} \left[\langle \epsilon | \mathcal{P} | \epsilon \rangle + 2 \langle \epsilon | \mathcal{S} | \delta \vec{R} \rangle + \langle \delta \vec{R} | \mathcal{M} | \delta \vec{R} \rangle \right] \quad (\text{S2})$$

where we use bra-ket notations to indicate summation over edges or nodes, \mathcal{P} projects the edge space to the subspace occupied by springs, $\mathcal{M} \equiv \mathcal{S}^t \mathcal{S} + \frac{k_w}{k} \mathcal{S}_w^t \mathcal{S}_w$ is the stiff matrix connecting the responding forces and displacements of nodes in an elastic network [61], and \bullet^t is our notation for the transpose of a matrix. Solving Eq.(S2), one finds the linear response,

$$|\delta \vec{R}\rangle = -\mathcal{M}^{-1} \mathcal{S}^t |\epsilon\rangle \quad (\text{S3})$$

which for a given mismatch field $|\epsilon\rangle$ minimizes the elastic energy in Eq.(1). Inserting Eq.(S3) back into the linear approximation Eq.(S2), we have [39]:

$$H(\Gamma) = \frac{k}{2} \langle \epsilon | \mathcal{P} - \mathcal{S} \mathcal{M}^{-1} \mathcal{S}^t | \epsilon \rangle = \frac{k}{2} \sum_{\Gamma} \epsilon_{\langle i,j \rangle} \mathcal{G}_{\langle i,j \rangle, \langle l,m \rangle} \epsilon_{\langle l,m \rangle} \quad (\text{S4})$$

with $\mathcal{G} = \mathcal{P} - \mathcal{S}(\mathcal{S}^t \mathcal{S} + \frac{k_w}{k} \mathcal{S}_w^t \mathcal{S}_w)^{-1} \mathcal{S}^t$, and $\epsilon_{\langle i,j \rangle} = \epsilon_{\gamma}$ for $\Gamma = \{\gamma \leftrightarrow \langle i,j \rangle\}$.

B. Density of states

We have shown the density of states converges to the one of mean-field networks [40]. Cooling strongly suppresses low frequency vibrational modes, as seen in Fig. S1. This temperature effects on density of states are primarily induced by the weak interactions: density of states changes little under cooling when $\alpha = 0$, as compared in (a) and (b) of Fig. S2. The slight change indicates that density of states is not independent of redundant constraints. However, when $\alpha > 0$, the low temperature density of states strongly differs from its high temperature counterpart, as shown in Fig. S2(a) and (c).

The modes diminished under cooling are localized vibrations. The participation ratio, $P(\omega) \equiv \frac{1}{Nd} (\sum_i \Psi_{\omega i}^2)^2 / \sum_i \Psi_{\omega i}^4$, quantifies the extensity of characteristic modes: $P \rightarrow 0$ corresponds to a localized mode, while $P \rightarrow 1$ means expanding over the system. Both low and high frequency ends of density of states are reduced under cooling, but the modes in the middle are enhanced, shown in the right panel of Fig. S1. This accords with

the small participation ratio of modes with low and high frequencies, see Fig. S2(d). In fact, all modes delocalize – the participation ratio increases over the whole spectrum – when the temperature decreases, shown in the inset of Fig. S1.

In addition to localization, another prominent feature of reduced low frequency modes is the power law diverging density of states $D(\omega) \sim \omega^{d-1}$, see Fig. S2. The abundance of low frequency localized modes appearing with a power law density of states characterizes “fractons” near the rigidity percolation [45, 62, 63]. The exponent of the diverging tail, in Fig. S2(a), implies the fracton dimension $d \approx 0.75$, which is consistent with 0.78 observed for the rigidity percolation [63, 64]. Different fracton dimension d is observed for different coordination number in the case of rigidity window shown in Fig. S2(b).

We discuss when the temperature affects the mode with frequency ω in Section C and show illustrations of “fractons” in Section D.

C. Adaptation effects on density of states

When $\alpha > 0$, following Eq.(6), we see the typical elastic energy corresponding to a mode of frequency ω scales as $\alpha/(\omega^2 + \alpha)$, which is proportional to α for $\omega \sim 1$, while proportional to 1 when $\omega \ll \sqrt{\alpha}$. This implies that the elastic energy in the degrees of freedom corresponding to the modes of low frequency is of the same magnitude as the one in the redundant constraints. Similar to the redundant constraints, these low frequency modes are reduced under cooling.

From Eq.(12b), $T^*(\omega, \alpha) \sim \alpha/(\omega^2 + \alpha)$ gives an estimate on the temperature scale the mode ω begins to be reduced. The adaptation effect at this temperature scale can be seen in the right panel of Fig. S1. For example, the green line at $T \approx 0.04 \ll 1$ shows a density of states with

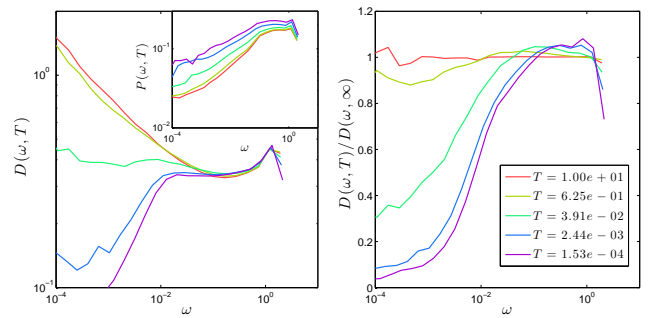


FIG. S1: Variation of density of states $D(\omega, T)$ with temperature for the same $z = -0.055$, $\alpha = 0.0003$. Left: density of states in log-log scale. Right: density of states normalized by its $T = \infty$ value, emphasizing its difference under cooling. Inset: participation ratio $P(\omega, T)$ variation under cooling.

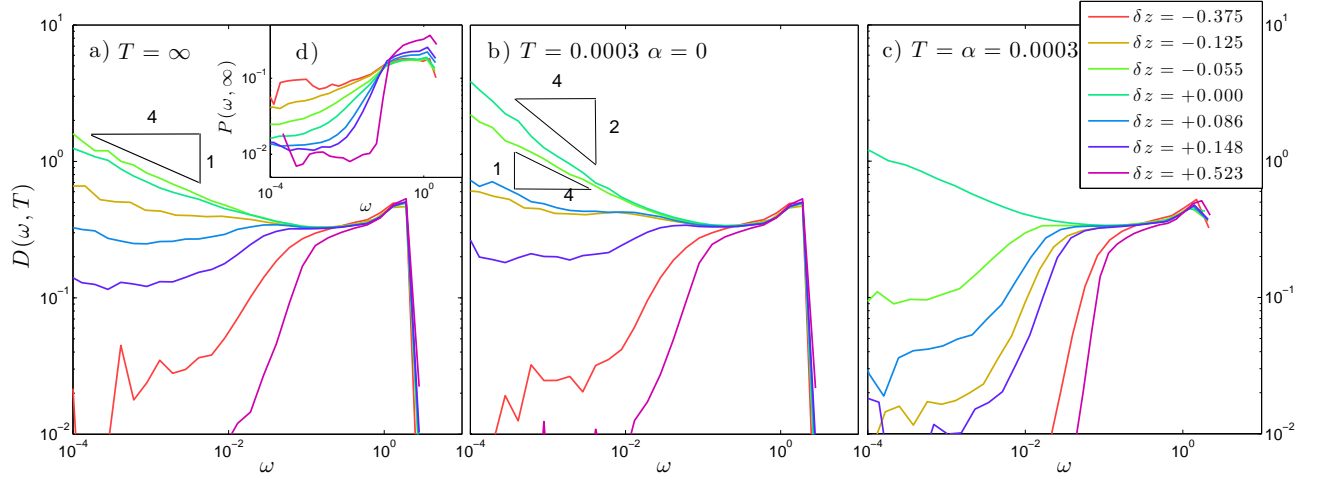


FIG. S2: Density of states $D(\omega, T)$ for adaptive networks with different z . (a) Random diluted networks $T = \infty$; a power law $D(\omega) \sim \omega^{-0.25}$ is shown in low frequency range for networks near z_{cen} . (b) Adaptive networks without weak constraints ($\alpha = 0$) at $T = 0.0003$; power laws with different exponents are shown for networks in the rigidity window: $D(\omega) \sim \omega^{-0.25}$ for $\delta z = -0.055$, $D(\omega) \sim \omega^{-0.5}$ for $\delta z = 0.0$. (c) Adaptive networks with weak constraints ($\alpha = 0.0003$) at $T \approx \alpha$; away from isostatic, density of states are gapped between zero frequency and Boson peak, where $D(\omega) \sim \omega^0$. Inset (d) Participation ratio $P(\omega, T)$ at $T = \infty$, see text for definition.

frequencies $\omega \lesssim \sqrt{\alpha} \approx 0.01$ strongly suppressed, while the shape of density of states with $\omega \approx 0.1$ and above is almost unchanged. The purple line, $T \approx 10^{-4} \sim \alpha$, shows a density of states whose highest frequency $\omega \sim 1$ is also significantly reduced.

D. Fractons

“Fractons” are different from either the low frequency Debye modes or the anomalous modes on the boson peak, as shown in Fig. S3. The “fractons” (Fig. S3(c)) are localized and random compared to the Debye modes (Fig. S3(a)), and concentrated on fractal sets with sharp boundaries, unlike the extended anomalous modes (Fig. S3(b)). The “fractons” correspond to the collective modes of large isostatic or nearly isostatic regions, shown in Fig. S4.

E. Vibrational entropy contribution

In addition to the random network model, the structure and sequentially the elastic potential evolve with

temperature in the liquid phase of the adaptive network model. Freezing into a glass phase eliminates this variability and leads to a contribution to the jump of specific heat [65]. We estimate this contribution from vibrations in this subsection.

The vibrational entropy includes both linear $\omega > 0$ and floppy $\omega = 0$ vibration modes [65]:

$$s_{vib}(T) = [1 - n_r(T)] \int d\omega D(\omega, T) \ln \frac{eT}{\hbar\omega} + f(T) \ln \Lambda \quad (\text{S5})$$

Λ sets a cutoff volume for floppy modes, which is approximately the atomic spacing measured in the Lindemann’s length: $\Lambda \approx (1/0.15)^d$, of order 10^3 in 3D [55]. f is the floppy mode density, dual to the number of redundant constraints density $f(T) = -\delta z/z + n_r(T)$ and thus $\partial f(T)/\partial T = \partial n_r(T)/\partial T$. The jump of specific heat,

$$\Delta c_{vib} = T_g \frac{\partial n_r(T)}{\partial T} \bigg|_{T_g} \left[\ln \Lambda - \int d\omega D_{T_g}(\omega) \ln \frac{eT_g}{\hbar\omega} \right] + [1 - n_r(T_g)] \int d\omega T_g \frac{\partial D_T(\omega)}{\partial T} \bigg|_{T_g} \ln \frac{eT_g}{\hbar\omega} \quad (\text{S6})$$

The derivatives on $\ln T$ in Eq.(S5), continuous in the glass

transition, have been subtracted.

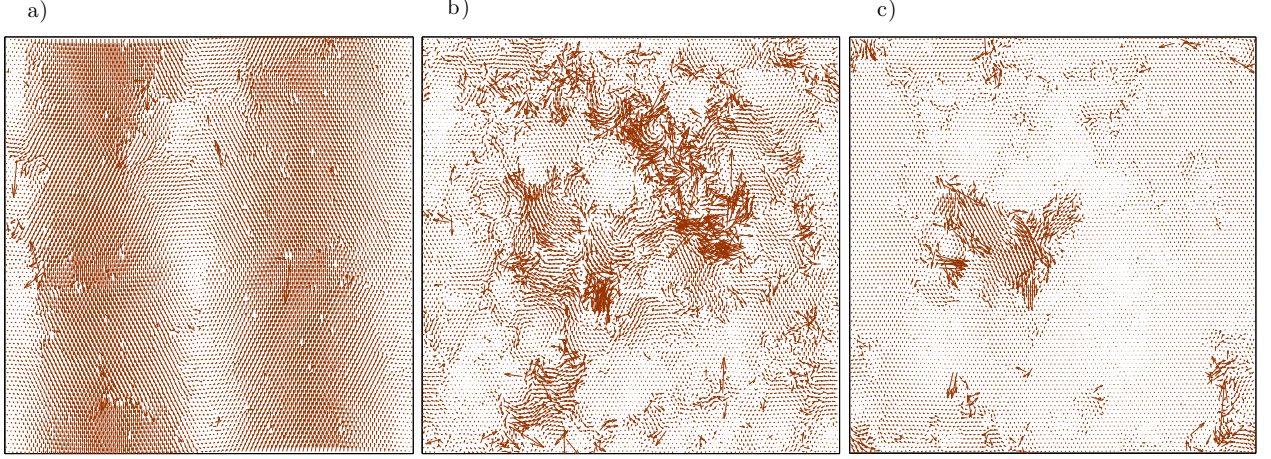


FIG. S3: Vector plots of vibrational modes in randomly diluted networks, $N = 100 \times 100$. (a) A typical Debye mode, $\delta z = 0.501$, $\omega = 0.017$. (b) A typical anomalous mode on boson peak, $\delta z = -0.049$, $\omega = 0.011$. (c) A typical fracton, $\delta z = -0.049$, $\omega = 0.0007$.

We estimate the upper limit of the vibrational contribution. ① The first term in Eq.(S6): Debye frequency ω_D sets the upper limit of the integral in the bracket, $-\ln(eT_g/\hbar\omega_D)$. As the glass transition temperature T_g and Debye temperature $\theta_D = \hbar\omega_D/k_B$ are usually of the same order, the bracket in the first term is dominated by $\ln\Lambda$. From Eqs.(11), we have $\partial n_r/\partial \ln T|_{T_g} \approx \frac{1}{2}n_{ex}(T_g) \lesssim \frac{1}{2}n_0\sqrt{T_g} \lesssim 0.02\sqrt{\alpha}$, and $\ln\Lambda \approx 5$ in 2D. Compared to the specific heat values, which are of order one shown in Fig. 7, and the scalings of the minima $-0.1/\ln\alpha$ given in [39], the contribution, $0.1\sqrt{\alpha}$, is insignificant if $0 < \alpha < 0.1$.

② The second term in Eq.(S6): The upper limit of the bracket is 1. Replacing $\ln(eT/\hbar\omega)$ with its upper limit $\ln\Lambda$, we simplify the integral to $\int d\omega T \partial D/\partial T$. We can estimate the upper limit of the derivative in the integral approximately by $\Delta n_T/\Delta \ln T$, where Δn_T is the number density of the modes reduced under cooling. $\Delta n_T \approx 0.2 \int_0^{0.01} \omega^{-0.25} d\omega \approx 0.01$, roughly the number fraction of “fractons” suppressed under cooling. Together, the upper limit of the contribution of the second term is $\Delta n_T/\ln 10 \times \ln\Lambda \approx 0.03$, moderate compared to the values of order one.

Therefore, the vibrational entropy contributes mildly to the jump of specific heat, and does not change the qualitative behavior of Δc in network glasses. In other glasses, where the number of constraints depends on the temperature [66, 67], the vibrational entropy may dominate the contribution to the jump of specific heat and the dynamics is very fragile [65].

-
- [1] P. G. Debenedetti and F. H. Stillinger, *Nature* **410**, 259 (2001).
 - [2] F. H. Stillinger and T. A. Weber, *Science*(Washington, DC) **225**, 983 (1984).
 - [3] G. Adam and J. H. Gibbs, *The Journal of Chemical Physics* **43**, 139 (1965).

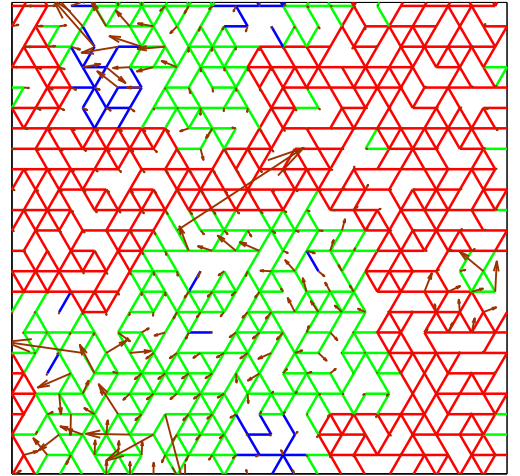


FIG. S4: Correlation between a low frequency fractal mode and isostatic clusters. A network configuration ($\delta z = -0.042$) is shown with its springs in the over-constrained regions colored in red, in the isostatic regions colored in green, and in the floppy regions colored in blue. A typical fracton ($\omega = 5 \times 10^{-4}$) specified in this configuration is plotted on top.

- [4] T. R. Kirkpatrick, D. Thirumalai, and P. G. Wolynes, *Phys. Rev. A* **40**, 1045 (1989).
- [5] V. Lubchenko and P. G. Wolynes, *Annual Review of Physical Chemistry* **58**, 235 (2007).
- [6] J.-P. Bouchaud and G. Biroli, *The Journal of Chemical Physics* **121**, 7347 (2004).
- [7] R. V. Chamberlin, *Phys. Rev. Lett.* **82**, 2520 (1999).
- [8] J. C. Dyre and N. B. Olsen, *Physical Review E* **69**, 042501 (2004).
- [9] D. Chandler and J. P. Garrahan, arXiv preprint arXiv:0908.0418 (2009).
- [10] L.-M. Martinez and C. A. Angell, *Nature* **410**, 663 (2001).
- [11] L.-M. Wang, C. A. Angell, and R. Richert, *The Journal of Chemical Physics* **125**, 074505 (2006).
- [12] R. W. Hall and P. G. Wolynes, *Phys. Rev. Lett.* **90**, 085505 (2003).
- [13] D. Bezenko and V. Lubchenko, *The Journal of Physical Chemistry B* **113**, 16337 (2009).
- [14] P. Rabochiy and V. Lubchenko, *The Journal of chemical physics* **138**, 12A534 (2013).
- [15] A. Anderson, *Amorphous Solids: Low Temperature Properties*, edited by W. A. Phillips, Topics in Current Physics, Vol. 24 (Springer, Berlin, 1981).
- [16] K. Ngai, A. Sokolov, and W. Steffen, *Journal of Chemical Physics* **107**, 5268 (1997).
- [17] V. N. Novikov, Y. Ding, and A. P. Sokolov, *Phys. Rev. E* **71**, 061501 (2005).
- [18] M. Tatsumisago, B. L. Halfpap, J. L. Green, S. M. Lindsay, and C. A. Angell, *Phys. Rev. Lett.* **64**, 1549 (1990).
- [19] W. A. Kamitakahara, R. L. Cappelletti, P. Boolchand, B. Halfpap, F. Gompf, D. A. Neumann, and H. Mutka, *Phys. Rev. B* **44**, 94 (1991).
- [20] D. Selvanathan, W. Bresser, P. Boolchand, and B. Goodman, *Solid State Communications* **111**, 619 (1999).
- [21] J. Maxwell, *Philos. Mag.* **27**, 294 (1864).
- [22] J. Phillips, *Journal of Non-Crystalline Solids* **34**, 153 (1979).
- [23] J. C. Phillips and M. F. Thorpe, *Sol. State Comm.* **53**, 699 (1985).
- [24] R. Böhmer and C. A. Angell, *Phys. Rev. B* **45**, 10091 (1992).
- [25] M. Micoulaut and P. Boolchand, *Phys. Rev. Lett.* **91**, 159601 (2003).
- [26] K. O. Trachenko, M. T. Dove, M. J. Harris, and V. Heine, *Journal of Physics: Condensed Matter* **12**, 8041 (2000).
- [27] C. S. O'Hern, L. E. Silbert, A. J. Liu, and S. R. Nagel, *Phys. Rev. E* **68**, 011306 (2003).
- [28] P. Chen, C. Holbrook, P. Boolchand, D. G. Georgiev, K. A. Jackson, and M. Micoulaut, *Phys. Rev. B* **78**, 224208 (2008).
- [29] K. Chen, W. G. Ellenbroek, Z. Zhang, D. T. Chen, P. J. Yunker, S. Henkes, C. Brito, O. Dauchot, W. Van Saarloos, A. J. Liu, *et al.*, *Physical review letters* **105**, 025501 (2010).
- [30] A. Ghosh, V. K. Chikkadi, P. Schall, J. Kurchan, and D. Bonn, *Physical review letters* **104**, 248305 (2010).
- [31] M. Wyart, L. E. Silbert, S. R. Nagel, and T. A. Witten, *Physical Review E* **72**, 051306 (2005).
- [32] M. Wyart, *Annales de Phys* **30**, 1 (2005).
- [33] N. Xu, M. Wyart, A. J. Liu, and S. R. Nagel, *Physical review letters* **98**, 175502 (2007).
- [34] C. Brito and M. Wyart, *The Journal of Chemical Physics* **131**, 024504 (2009).
- [35] E. DeGiuli, A. Laversanne-Finot, G. A. Düring, E. Lerner, and M. Wyart, *Soft Matter* **10**, 5628 (2014).
- [36] E. DeGiuli, E. Lerner, C. Brito, and M. Wyart, *Proceedings of the National Academy of Sciences* **111**, 17054 (2014).
- [37] E. DeGiuli, E. Lerner, and M. Wyart, *The Journal of chemical physics* **142**, 164503 (2015).
- [38] S. Franz, G. Parisi, P. Urbani, and F. Zamponi, ArXiv e-prints (2015), arXiv:1506.01997 [cond-mat.dis-nn].
- [39] L. Yan, G. Düring, and M. Wyart, *Proceedings of the National Academy of Sciences* **110**, 6307 (2013).
- [40] L. Yan and M. Wyart, *Phys. Rev. Lett.* **113**, 215504 (2014).
- [41] W. G. Ellenbroek, V. F. Hagh, A. Kumar, M. F. Thorpe, and M. van Hecke, *Phys. Rev. Lett.* **114**, 135501 (2015).
- [42] C. F. Moukarzel, *Phys. Rev. E* **88**, 062121 (2013).
- [43] D. J. Jacobs and M. F. Thorpe, *Phys. Rev. Lett.* **80**, 5451 (1998).
- [44] P. M. Duxbury, D. J. Jacobs, M. F. Thorpe, and C. Moukarzel, *Phys. Rev. E* **59**, 2084 (1999).
- [45] S. Feng and P. N. Sen, *Phys. Rev. Lett.* **52**, 216 (1984).
- [46] D. J. Jacobs and M. F. Thorpe, *Phys. Rev. Lett.* **75**, 4051 (1995).
- [47] M. Thorpe, D. Jacobs, M. Chubynsky, and J. Phillips, *Journal of Non-Crystalline Solids* **266-269**, Part 2, 859 (2000).
- [48] M. V. Chubynsky, M.-A. Brière, and N. Mousseau, *Phys. Rev. E* **74**, 016116 (2006).
- [49] M.-A. Brière, M. V. Chubynsky, and N. Mousseau, *Phys. Rev. E* **75**, 056108 (2007).
- [50] M. Micoulaut and J. C. Phillips, *Phys. Rev. B* **67**, 104204 (2003).
- [51] We have tested the validity of the linear approximation: the energy difference from the steepest decent results keeps below 3% for $\epsilon < 0.02$.
- [52] See the Supplemental Material at , which includes Refs. [61–67], for the formalism of elastic energy, temperature dependence of density of states, images of fractons, and the vibrational entropy contribution of specific heat.
- [53] J. Barré, *Phys. Rev. E* **80**, 061108 (2009).
- [54] D. J. Jacobs and B. Hendrickson, *Journal of Computational Physics* **137**, 346 (1997).
- [55] F. Lindemann, “*Phys. z.*, 11, 609 (1910),” (1912).
- [56] A different coefficient used, as the number of Monte Carlo steps is 1000 times longer.
- [57] B. Derrida, *Phys. Rev. B* **24**, 2613 (1981).
- [58] M. a. Mézard, *Information, Physics and Computation* (Oxford University press, 2009).
- [59] M. Wyart, H. Liang, A. Kabla, and L. Mahadevan, *Phys. Rev. Lett.* **101**, 215501 (2008).
- [60] G. Düring, E. Lerner, and M. Wyart, *Soft Matter* **9**, 146 (2013).
- [61] C. Calladine, *International Journal of Solids and Structures* **14**, 161 (1978).
- [62] S. Alexander and R. Orbach, *J. Phys. (Paris) Lett.* **43**, 625 (1982).
- [63] T. Nakayama, K. Yakubo, and R. L. Orbach, *Rev. Mod. Phys.* **66**, 381 (1994).
- [64] S. Feng, *Phys. Rev. B* **32**, 5793 (1985).
- [65] M. Wyart, *Phys. Rev. Lett.* **104**, 095901 (2010).
- [66] P. K. Gupta and J. C. Mauro, *The Journal of Chemical Physics* **130**, 094503 (2009).
- [67] M. Bauchy and M. Micoulaut, *Journal of Non-Crystalline Solids* **357**, 2530 (2011).